

Two-loop corrections to the decay rate of parapositronium

Gregory S. Adkins* and Nathan M. McGovern

Franklin & Marshall College, Lancaster, Pennsylvania 17604

Richard N. Fell†

Brandeis University, Waltham, Massachusetts 01742

J. Sapirstein‡

University of Notre Dame, Notre Dame, Indiana 46556

(Dated: March 25, 2022)

Abstract

Order α^2 corrections to the decay rate of parapositronium are calculated. A QED scattering calculation of the amplitude for electron-positron annihilation into two photons at threshold is combined with the technique of effective field theory to determine an NRQED Hamiltonian, which is then used in a bound state calculation to determine the decay rate. Our result for the two-loop correction is 5.1243(33) in units of $(\alpha/\pi)^2$ times the lowest order rate. This is consistent with but more precise than the result 5.1(3) of a previous calculation.

PACS numbers: 36.10.Dr, 06.20.Jr, 12.20.Ds, 31.30.Jv

*gadkins@fandm.edu

†fell@brandeis.edu

‡jsapirst@nd.edu

I. INTRODUCTION

Effective field theories have proved to be a powerful tool in a variety of applications, ranging over areas as diverse as nuclear physics [1], lattice QCD [2], heavy flavor physics [3], and Bose-Einstein condensation [4]. One of the first applications of the technique [5] was to the bound state problem in Quantum Electrodynamics (QED). As the approach incorporates QED effects as perturbations to a nonrelativistic Schrödinger problem, it is known as nonrelativistic QED (NRQED).

Effective field theories in general provide a way of treating physics that involves multiple scales. Specifically in the case of atomic physics, NRQED deals with the fact that three scales—the rest mass of the electron, m ; the average three-momentum of an electron, $m\alpha$; and the electron binding energy, $m\alpha^2$ —all play significant roles in radiative and recoil corrections. While the Bethe-Salpeter equation [6] or three-dimensional variants of it [7, 8, 9] provide a consistent framework to carry out calculations of atomic properties, the implementation is sufficiently complicated so that while first-order calculations were carried out in the early 1950's for a number of systems, the next order calculations were not completely evaluated for over 40 years.

This situation has radically changed since the introduction of effective field theory techniques for QED bound state calculations. A set of calculations using various implementations of NRQED that complete the evaluation of order α^4 Rydbergs energy shifts have been carried out over the last few years: we note progress in helium [10], positronium [11], and muonium [12]. In addition to this work on energy levels, the order α^2 corrections to the decay rate of orthopositronium [13] and parapositronium [14] have also been treated using NRQED.

In this paper we will be concerned with the latter decay rate, $\Gamma_{p\text{-Ps}}$. The dominant decay mode of $p\text{-Ps}$ is into two photons, and the associated decay rate was found by Wheeler [15] and Pirenne [16] to be

$$\Gamma_{p\text{-Ps}}^{(0)}(2\gamma) = \frac{1}{2} \frac{mc^2}{\hbar} \alpha^5 = 2\pi c R_\infty \alpha^3 = 8032.5028(1) \mu s^{-1}. \quad (1)$$

The numerical value is determined using the 1998 CODATA adjustment of constants [17], with the 12 ppb uncertainty dominated by the uncertainty in the fine structure constant. In the following we will refer to this lowest order result simply as Γ_0 .

The lowest order rate differs by 0.52 percent from the most accurate measurement [18], which determines

$$\Gamma_{p\text{-Ps}}^{exp} = 7990.9(1.7)\mu\text{s}^{-1}. \quad (2)$$

The bulk of the difference is accounted for by the one-loop corrections to the decay rate, calculated by Harris and Brown [19], which change the theoretical prediction by 0.59 percent to

$$\Gamma(1\text{loop}) = \Gamma_0 \left\{ 1 + \frac{\alpha}{\pi} \left(\frac{\pi^2}{4} - 5 \right) \right\} = 7985.249\mu\text{s}^{-1}. \quad (3)$$

The residual 0.07 percent discrepancy corresponds to a three standard deviation difference between experiment and theory at the one loop order, and is of a size compatible with order α^2 corrections.

Corrections of this order arise both from two-loop corrections—the subject of this paper—and from the four photon decay of p -Ps. The experiment [18] measures the total decay rate of p -Ps, which in QED includes decays into any even number of photons. We note that exotic interactions could allow decay into an odd number of photons, and experiments looking for this kind of decay have put limits on the branching ratio arising from such interactions, specifically 2.8×10^{-6} for $p\text{-Ps} \rightarrow 3\gamma$ [20] and 2.7×10^{-7} for $p\text{-Ps} \rightarrow 5\gamma$ [21]. The only effect that contributes at a non-negligible level is four-photon decay, which was first calculated in Ref. [22]. The highest accuracy determination of the rate, along with a calculation of first-order radiative corrections to it, is given in Ref. [23], where references to other calculations can be found. The result is

$$\Gamma_{p\text{-Ps}}(4\gamma) = 0.274290(8) \left(\frac{\alpha}{\pi} \right)^2 \Gamma_0 \left\{ 1 - 14.5(6) \left(\frac{\alpha}{\pi} \right) \right\}. \quad (4)$$

While this effect is well under the present level of experimental precision, we will include it in our final prediction.

The remaining contribution from two and higher loops can be parameterized via

$$\Gamma_{p\text{-Ps}}(2+\text{loop}) = \Gamma_0 \left\{ -2\alpha^2 \ln \alpha + B_{2\gamma} \left(\frac{\alpha}{\pi} \right)^2 - \frac{3\alpha^3}{2\pi} \ln^2 \alpha + C \frac{\alpha^3}{\pi} \ln \alpha + D \left(\frac{\alpha}{\pi} \right)^3 \right\}. \quad (5)$$

The $O(\alpha^2)$ logarithmic term was calculated in Ref. [24], and the leading $O(\alpha^3)$ logarithm in Ref. [25]. The coefficient of the subleading $O(\alpha^3)$ logarithmic term

$$C = -\frac{\pi^2}{2} + 10 \ln 2 + \frac{533}{90} = 7.9189 \quad (6)$$

is also now well-established, with three different groups [26, 27, 28] in agreement. The terms of order $\alpha^3\Gamma_0$ are well below the experimental accuracy, but will be included in our final tally. The leading logarithmic term removes almost all the residual 0.07 percent discrepancy, so as long as the constant $B_{2\gamma}$ is not too large, theory and experiment are in agreement. The experimental error corresponds to a value of 39 for $B_{2\gamma}$. Nevertheless, a direct calculation of this constant is desirable, both because it is possible that the constant is large, as is frequently the case in QED bound state calculations, and for comparison with future experiments of higher precision. As mentioned above, this calculation has been recently carried out using effective field theory techniques by Czarnecki, Melnikov, and Yelkhovsky [14], referred to here as CMY. After correction of one part of their calculation [29], their result is

$$B_{2\gamma} = 5.1(3). \quad (7)$$

This gives for the total theory, including the four-photon decay, the prediction

$$\Gamma_{p\text{-Ps}}^{th}(\text{CMY}) = 7989.616(13)\mu s^{-1}, \quad (8)$$

which is in good agreement with experiment. The principal result of this paper is the confirmation of the previous calculation, but with higher precision,

$$B_{2\gamma} = 5.1243(33), \quad (9)$$

which leads to our main result,

$$\Gamma_{p\text{-Ps}}^{th} = 7989.6178(2)\mu s^{-1}. \quad (10)$$

The plan of this paper is the following. In section II we explain our implementation of NRQED, which differs significantly from that of CMY. In section III we carry out a QED calculation of the scattering amplitude at threshold to two loops. In the concluding section we use this amplitude in a bound state calculation to determine $B_{2\gamma}$, and we discuss the related o -Ps decay rate calculation.

II. NONRELATIVISTIC QUANTUM ELECTRODYNAMICS

The basic idea of NRQED is to take advantage of the fact that many of the complexities of QED are associated with the scale of the electron Compton wavelength, which in an

atomic bound state is effectively a point interaction, so that in a bound state calculation one can account for most QED effects by introducing a delta function potential along with the usual relativistic perturbations. However, ultraviolet divergences are present when these interactions are treated in higher order, and the regularization of these divergences can be done in different ways. In addition, when carrying out scattering calculations, the infinite range of the Coulomb interaction leads to infrared divergences that can also be regularized in different ways. For these reasons, the details of an NRQED calculation can be quite different when done by different groups. We consider this to be an advantage, as agreement between different methods, such as will be found here, lends support to the reliability of these complex calculations.

CMY handled both ultraviolet and infrared divergences with dimensional regularization. In the present work, we only use dimensional regularization to handle ultraviolet divergences in the QED scattering calculation of section III. We regulate infrared divergences by introducing a photon mass $\tilde{\lambda} = m\lambda$, and we cut off ultraviolet divergences in the NRQED calculation with a maximum loop three-momentum Λ .

A detailed description of NRQED applied to the decay rate of orthopositronium can be found in Ref. [13]. A great deal of the analysis given there applies equally well to parapositronium, but for completeness we give here a complete, but somewhat abbreviated, discussion, referring the reader interested in more details to Ref. [13].

Because we regulate infrared infinities with a photon mass, it is necessary to set up a consistent set of interactions that incorporate this effect. These interactions are most conveniently expressed in the center-of-mass frame in momentum space, with an incoming electron momentum \vec{k} and an outgoing electron momentum \vec{l} . It is also useful to define the frequently occurring denominators

$$D_\lambda(\vec{k}) = \vec{k}^2 + \tilde{\lambda}^2 \quad (11)$$

and

$$D_k = \vec{k}^2 + \gamma^2, \quad (12)$$

where $\gamma = m\alpha/2$. The NRQED interactions are depicted in Fig. 1.

At lowest order, the NRQED Hamiltonian consists of the usual nonrelativistic kinetic

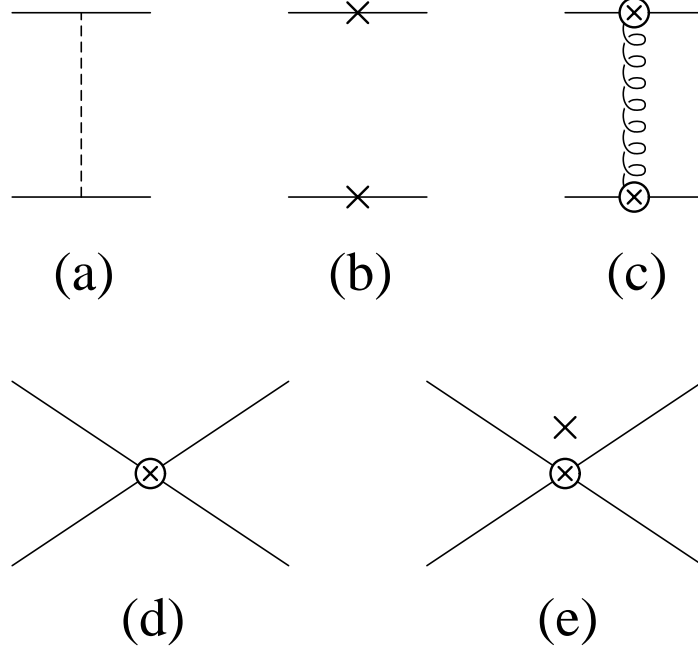


FIG. 1: The NRQED instantaneous potentials: (a) Coulomb, (b) relativistic mass increase, (c) Breit-Fermi, (d) four-fermion contact, (e) four-fermion derivative.

energy together with a modified Coulomb potential,

$$V_C(\vec{k}, \vec{l}) = -\frac{4\pi\alpha}{D_\lambda(\vec{k} - \vec{l})}. \quad (13)$$

The usual relativistic perturbations responsible for the fine structure of hydrogen are present, including the relativistic mass increase (RMI),

$$V_{RMI}(\vec{k}, \vec{l}) = -(2\pi)^3 \delta(\vec{k} - \vec{l}) \frac{\vec{k}^4}{4m^3} \quad (14)$$

and a term, which includes both relativistic corrections to the Coulomb potential and the exchange of a transverse photon, denoted V_{BF} . The full form of this “Breit-Fermi” interaction when a photon mass is present is

$$\begin{aligned} V_{BF}(\vec{k}, \vec{l}) = & -\frac{4\pi\alpha}{m^2} \left[\frac{|\vec{k} \times \vec{l}|^2 + \frac{1}{4}\tilde{\lambda}^2|\vec{k} + \vec{l}|^2}{D_\lambda^2(\vec{k} - \vec{l})} - \frac{(\vec{k} - \vec{l}) \times \vec{S}_- \cdot (\vec{k} - \vec{l}) \times \vec{S}_+}{D_\lambda(\vec{k} - \vec{l})} \right. \\ & \left. + \frac{3}{2}i \frac{(\vec{k} \times \vec{l}) \cdot (\vec{S}_- + \vec{S}_+)}{D_\lambda(\vec{k} - \vec{l})} - \frac{1}{4} \frac{|\vec{k} - \vec{l}|^2}{D_\lambda(\vec{k} - \vec{l})} \right]. \end{aligned} \quad (15)$$

It includes the Darwin term and the spin-orbit interaction, though we note the latter interaction does not contribute for S-states.

The next interaction we need for NRQED is the four-point interaction describing the decay process,

$$V_4(\vec{k}, \vec{l}) = V_4^0 \left\{ 1 + \frac{\alpha}{\pi} e_1 + \left(\frac{\alpha}{\pi} \right)^2 e_2 \right\} \quad (16)$$

where

$$V_4^0 = -\frac{2\pi\alpha^2}{m^2} i. \quad (17)$$

The constants e_1 and e_2 renormalize the interaction and will be determined from a matching calculation below. This interaction corresponds to a delta function in coordinate space and gives rise to an energy in which V_4 is multiplied by the square of the wave function at the origin, $m^3\alpha^3/8\pi$. The leading term is chosen so that the decay rate, given by $\Gamma = -2\text{Im}(E)$, reproduces the known lowest order result.

An important difference of the p -Ps calculation from the o -Ps calculation is the fact that the latter has a real contribution to V_4 arising from one-photon annihilation, a channel not available in the present case. The last interaction needed for the calculation accounts for the fact that the annihilation is not exactly pointlike, which leads to a derivative term,

$$V_{4der}(\vec{k}, \vec{l}) = \frac{4\pi\alpha^2}{3m^4} i(\vec{k}^2 + \vec{l}^2). \quad (18)$$

We note the relationship

$$V_{4der}(\vec{k}, \vec{l}) = -\frac{2}{3} V_4^0 \frac{\vec{k}^2 + \vec{l}^2}{m^2} \quad (19)$$

happens to be identical to the behavior of the interaction for o -Ps arising from one-photon exchange, which contributes to the hfs of positronium; this fact will be used below. We now describe how these interactions are used in a bound state NRQED calculation.

A. Bound state calculation

We now apply standard Rayleigh-Schrödinger perturbation theory to second order. (The corresponding diagrams are shown in Fig. 2.) We are interested only in imaginary contributions to the energy, so one factor of V_4 or V_{4der} must be present. The expression for first order perturbation theory in momentum space is

$$E_V^{(1)} = \int \frac{d^3p_2}{(2\pi)^3} \frac{d^3p_1}{(2\pi)^3} \phi^*(\vec{p}_2) V(\vec{p}_2, \vec{p}_1) \phi(\vec{p}_1), \quad (20)$$

where the wave function is

$$\phi(\vec{p}) = \left(\frac{\gamma^3}{\pi} \right)^{1/2} \frac{8\pi\gamma}{(\vec{p}^2 + \gamma^2)^2}. \quad (21)$$

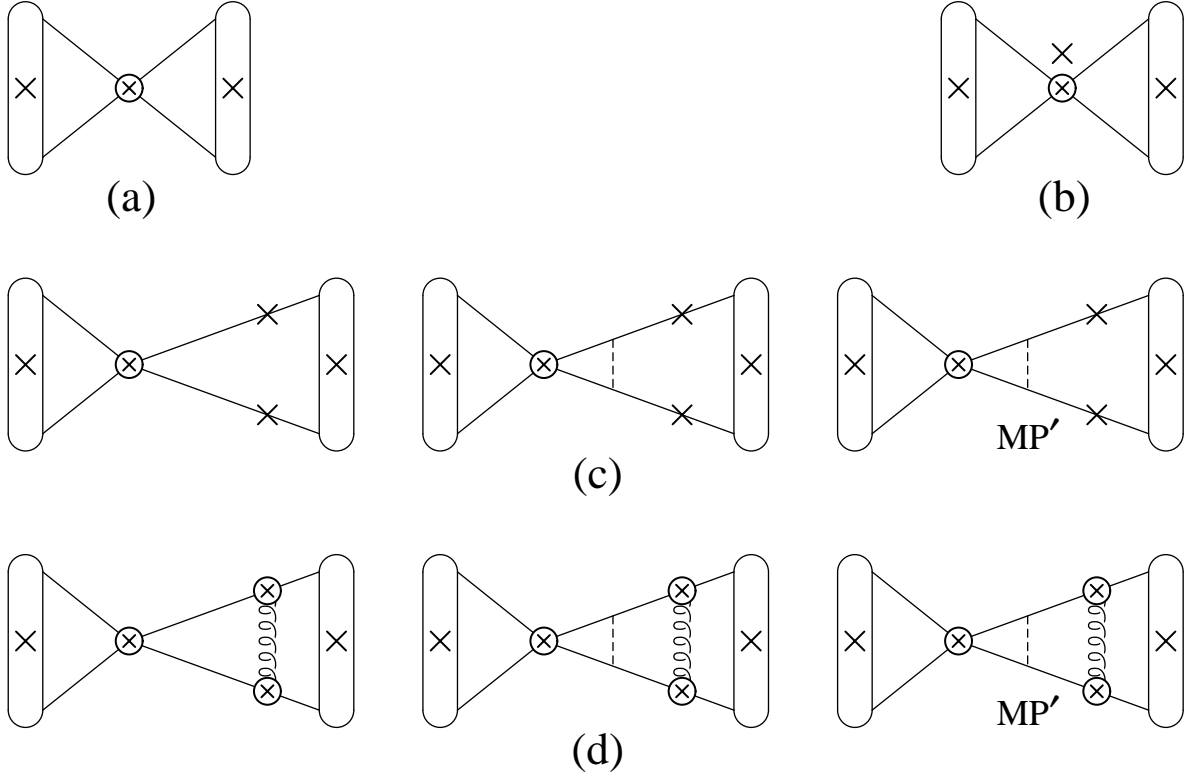


FIG. 2: First and second order bound state perturbation theory contributions to the energy shift. They are the first order (a) contact and (b) derivative contributions, and the second order (c) relativistic mass increase and (d) Breit-Fermi contributions. Contributions (c) and (d) are shown separated into their zero-, one-, and many-potential parts.

This gives the contributions

$$E_{V_4}^{(1)} = -\frac{i}{4}m\alpha^5 \left\{ 1 + \frac{\alpha}{\pi}e_1 + \left(\frac{\alpha}{\pi}\right)^2 e_2 \right\} \quad (22)$$

from Fig. 2a and

$$E_{V_{4der}}^{(1)} = \frac{2i\Lambda\alpha^6}{3\pi} - \frac{1}{4}im\alpha^7 \quad (23)$$

from Fig. 2b, where Λ is the maximum value allowed for the magnitude of the three-momentum $|\vec{p}_2|$ or $|\vec{p}_1|$.

In second order we need to evaluate expressions of the form

$$E_{ij}^{(2)} = \sum_{n \neq 0} \frac{\langle 0|V_i|n \rangle \langle n|V_j|0 \rangle}{E_0 - E_n}, \quad (24)$$

which can be written in terms of a reduced Coulomb Green's function,

$$E_{ij}^{(2)} = \frac{1}{(2\pi)^{12}} \int d^3p_2 d^3k d^3l d^3p_1 \phi^*(\vec{p}_2) V_i(\vec{p}_2, \vec{k}) G_R(\vec{k}, \vec{l}) V_j(\vec{l}, \vec{p}_1) \phi(\vec{p}_1). \quad (25)$$

The reduced Green's function in momentum space conveniently breaks into three parts, in which the electron either propagates freely, interacts once with a Coulomb potential, or interacts more than once. It is given by

$$G(\vec{k}, \vec{l}) = -(2\pi)^3 \delta^3(\vec{k} - \vec{l}) \frac{m}{D_k} - \frac{m}{D_k} \frac{4\pi\alpha}{|\vec{k} - \vec{l}|^2} \frac{m}{D_l} - R(\vec{k}, \vec{l}) \quad (26)$$

where

$$R(\vec{k}, \vec{l}) = \frac{32\pi m \gamma^3}{D_k^2 D_l^2} \left[\frac{5}{2} - \frac{4\gamma^2}{D_k} - \frac{4\gamma^2}{D_l} + \frac{1}{2} \ln A + \frac{2A - 1}{\sqrt{4A - 1}} \tan^{-1} \sqrt{4A - 1} \right], \quad (27)$$

with

$$A = \frac{D_k D_l}{4\gamma^2 |\vec{k} - \vec{l}|^2}. \quad (28)$$

When the interaction is a relativistic mass increase (see Fig. 2c), second order perturbation theory gives

$$E_{V_4, V_{RMI}}^{(2)} + E_{V_{RMI}, V_4}^{(2)} = -i \frac{\Lambda \alpha^6}{4\pi} - i \frac{m \alpha^7}{8} \ln\left(\frac{\Lambda}{2\gamma}\right) - i \frac{m \alpha^7}{32}, \quad (29)$$

and when it is a Breit-Fermi interaction (see Fig. 2d), the contribution is

$$E_{V_4, V_{BF}}^{(2)} + E_{V_{BF}, V_4}^{(2)} = -i \frac{\Lambda \alpha^6}{4\pi} - i \frac{3m \alpha^7}{8} \ln\left(\frac{\Lambda}{2\gamma}\right) - i \frac{7m \alpha^7}{16}, \quad (30)$$

where contributions of order $m \alpha^8$ and higher are dropped. A table of integrals useful in arriving at these results can be found in Ref. [13].

The final result for the NRQED bound state calculation is then

$$\Gamma_{\text{NRQED}} = \left\{ 1 + \frac{\alpha}{\pi} \left[e_1 - \frac{2\Lambda}{3m} \right] + \left(\frac{\alpha}{\pi} \right)^2 \left[e_2 + \frac{23\pi^2}{8} + 2\pi^2 \ln\left(\frac{\Lambda}{2\gamma}\right) \right] \right\} \Gamma_0, \quad (31)$$

which has been converted to a decay rate in the usual manner.

B. NRQED scattering calculation

The next step in the analysis is to consider the imaginary part of the amplitude in NRQED for Bhabha scattering at threshold. In lowest order this is simply V_4^0 , with no contribution from V_{4der} because of the presence of the momentum factors. Including the renormalization terms, we denote the overall effect of V_4 as

$$M_{\text{NRQED}}^{(0)} = V_4^0 \left\{ 1 + \frac{\alpha}{\pi} e_1 + \left(\frac{\alpha}{\pi} \right)^2 e_2 \right\}. \quad (32)$$

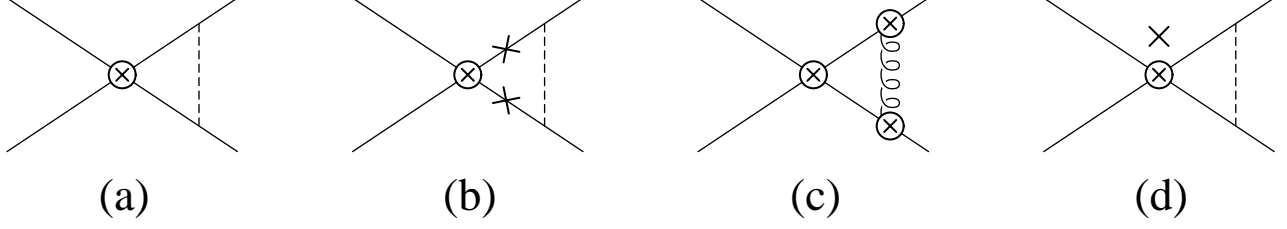


FIG. 3: The one-loop NRQED $e^-e^+ \rightarrow e^-e^+$ scattering graphs.

In first order, a simple calculation gives the contributions

$$M_{NRQED}^{(1)}(V_C) = \frac{\alpha}{\pi} V_4^0 \left(\frac{2\pi}{\lambda} \right) \left\{ 1 + \frac{\alpha}{\pi} e_1 \right\}, \quad (33)$$

$$M_{NRQED}^{(1)}(V_{RMI}) = \frac{\alpha}{\pi} V_4^0 \left(\frac{\Lambda}{m} - \frac{\pi\lambda}{2} \right), \quad (34)$$

$$M_{NRQED}^{(1)}(V_{BF}) = \frac{\alpha}{\pi} V_4^0 \left(\frac{\Lambda}{m} - \frac{\pi\lambda}{4} \right), \quad (35)$$

and

$$M_{NRQED}^{(1)}(V_{4der}) = \frac{\alpha}{\pi} V_4^0 \left(-\frac{8\Lambda}{3m} + \frac{4\pi\lambda}{3} \right), \quad (36)$$

shown in Fig. 3 a-d, which sum to

$$M_{NRQED}^{(1)} = \frac{\alpha}{\pi} V_4^0 \left(\frac{2\pi}{\lambda} \left\{ 1 + \frac{\alpha}{\pi} e_1 \right\} - \frac{2\Lambda}{3m} + \frac{7\pi\lambda}{12} \right). \quad (37)$$

In the next section we will require this amplitude equal the one-loop QED amplitude to determine e_1 . To determine e_2 a two-loop calculation is required. The calculation is almost identical to the scattering calculation carried out for hyperfine splitting in section 3 of Ref. [13], where twelve diagrams (labeled a-l) were analyzed. The last two of them, k and l , involved a real contribution to V_4 not present for p -Ps, so they are dropped. The other ten (see Fig. 4) are all proportional to the lowest order amplitude and can be taken over directly to p -Ps by simply using the lowest order amplitude for p -Ps instead of hfs. The only other change needed is the modification of the three diagrams which involve the V_{BF} interaction, which is different for the two states. However, the difference is simply

$$\delta V_{BF} = -\frac{8\pi\alpha}{3m^2} \frac{|\vec{k} - \vec{l}|^2}{D_\lambda(\vec{k} - \vec{l})}, \quad (38)$$

which leads to the modifications

$$\delta f = \left(\frac{\alpha}{\pi} \right)^2 V_4^0 \left(\frac{8\pi\Lambda}{3\tilde{\lambda}} - \frac{4\pi^2 \ln 2}{3} \right), \quad (39)$$

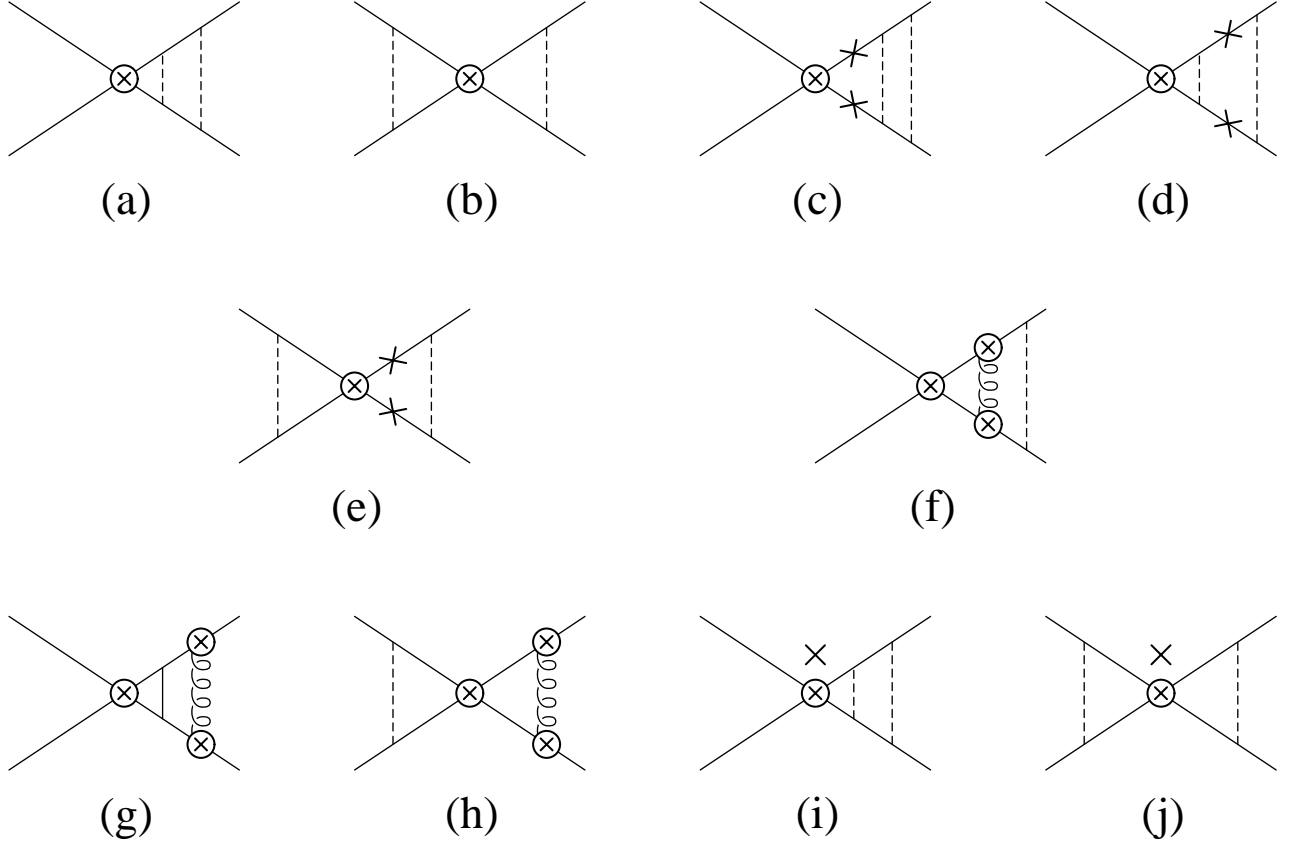


FIG. 4: The two-loop NRQED $e^-e^+ \rightarrow e^-e^+$ scattering graphs.

$$\delta g = \left(\frac{\alpha}{\pi}\right)^2 V_4^0 \frac{4\pi^2}{3} \ln\left(\frac{\Lambda}{2\tilde{\lambda}}\right), \quad (40)$$

and

$$\delta h = \left(\frac{\alpha}{\pi}\right)^2 V_4^0 \left(\frac{8\pi\Lambda}{3\tilde{\lambda}} - \frac{4\pi^2}{3}\right). \quad (41)$$

Finally, graphs i and j are derivative terms, but as mentioned earlier, the ratio of the derivative term to the lowest order matrix element is the same for hfs as it is for p -Ps, so the results from Ref. [13] can be taken over directly. The final result for the two-loop contribution to threshold scattering is

$$M_{NRQED}^{(2)} = \left(\frac{\alpha}{\pi}\right)^2 V_4^0 \left(\frac{\pi^2(2\ln 2 + 1)}{\lambda^2} - \frac{4\pi\Lambda}{3\tilde{\lambda}} + 2\pi^2 \ln\left(\frac{\Lambda}{2\tilde{\lambda}}\right) + \frac{4\pi^2}{3}\right), \quad (42)$$

and the NRQED amplitude that is to be compared to the QED scattering calculation is

$$M_{NRQED} = M_{NRQED}^{(0)} + M_{NRQED}^{(1)} + M_{NRQED}^{(2)}. \quad (43)$$

III. QED SCATTERING CALCULATION

We are interested in the imaginary part of the scattering amplitude for an electron and positron to annihilate into two photons, and the two photons then to create an electron and positron. While this amplitude at threshold is simply a constant, in order to determine the derivative term in NRQED we also need the behavior slightly above threshold. If we assign the momentum \vec{k} to the incoming electron and \vec{l} to the outgoing electron, with the positrons having opposite momentum, a straightforward calculation leads to the above-threshold matrix element

$$M_{QED}^{(0)}(\vec{k}, \vec{l}) = V_4^0 \left(1 - \frac{2}{3} \frac{\vec{k}^2 + \vec{l}^2}{m^2} \right). \quad (44)$$

This requires that NRQED have the forms for V_4 and V_{4der} used in the previous section. At threshold we have simply

$$M_{QED}^{(0)} = V_4^0. \quad (45)$$

We will follow the convention of listing results for a given n -loop contribution to the scattering amplitude

$$M_{QED}^{(n)} = \left(\frac{\alpha}{\pi} \right)^n V_4^0 I^{(n)} \quad (46)$$

by giving I instead of the full amplitude. So for the zero-loop contribution we have

$$I^{(0)} = 1. \quad (47)$$

Continuing to the one-loop calculation, there are three diagrams that must be considered, which we call the self-energy (SE), vertex (V), and ladder (L). They are shown in Fig. 5. The self-energy and vertex results are

$$I_{SE} = 2 \ln \lambda + 4 \ln 2 + 1 + O(\lambda), \quad (48)$$

and

$$I_V = -4 \ln \lambda + \frac{\pi^2}{4} - 4 \ln 2 - 4 + O(\lambda). \quad (49)$$

The infrared logarithms present in I_{SE} and I_V are artifacts of the renormalization process. The ladder diagram has an infrared singularity associated with binding that we denote as I_B , defined by

$$I_B = \frac{\pi}{\lambda} + \ln \lambda - 1 - \frac{\pi \lambda}{8} + O(\lambda^2). \quad (50)$$

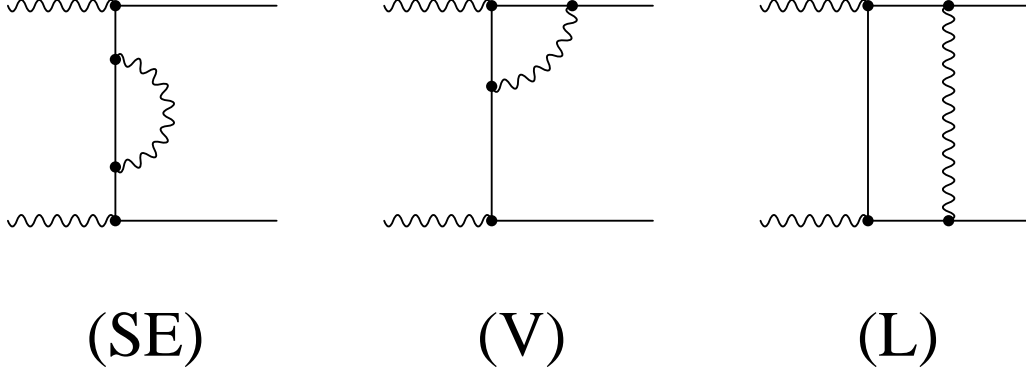


FIG. 5: One-loop QED graphs contributing to the parapositronium decay rate. They are (SE) the self-energy graph, (V) the vertex graph, and (L) the ladder graph.

The ladder diagram turns out to be proportional to I_B , which will also prove a useful factor in the two-loop calculation. We find

$$I_L = 2I_B + O(\lambda). \quad (51)$$

A simple summation of the one-loop contributions gives the overall result

$$I^{(1)} = \frac{2\pi}{\lambda} + A(\lambda), \quad (52)$$

with

$$A(\lambda) = \frac{\pi^2}{4} - 5 + E\lambda. \quad (53)$$

Here $E\lambda$ represents the uncalculated order λ contribution. The value of E does not affect the final result.

The two-loop calculation involves eight sets of graphs. In this part of the calculation ultraviolet divergences are regulated by working in $n = 4 - 2\epsilon$ dimensions. When doing so a common factor of $[(4\pi\mu^2/m^2)e^{-\gamma_E}]^{2\epsilon}$ is always present (where μ is a mass scale introduced in the process of dimensional regularization, and γ_E is the Euler gamma constant), but we leave it unwritten. It can be taken to unity after renormalization.

We begin the discussion with two-loop corrections to a photon vertex, shown in Fig. 6a. In diagrams a2 and a5 the self-energy subdiagram is understood to be accompanied by a self-mass counterterm. This convention differs from CMY, but we have been able to show agreement with their results if the counterterm is included. The unrenormalized results are given in Table I. The total class a unrenormalized result is

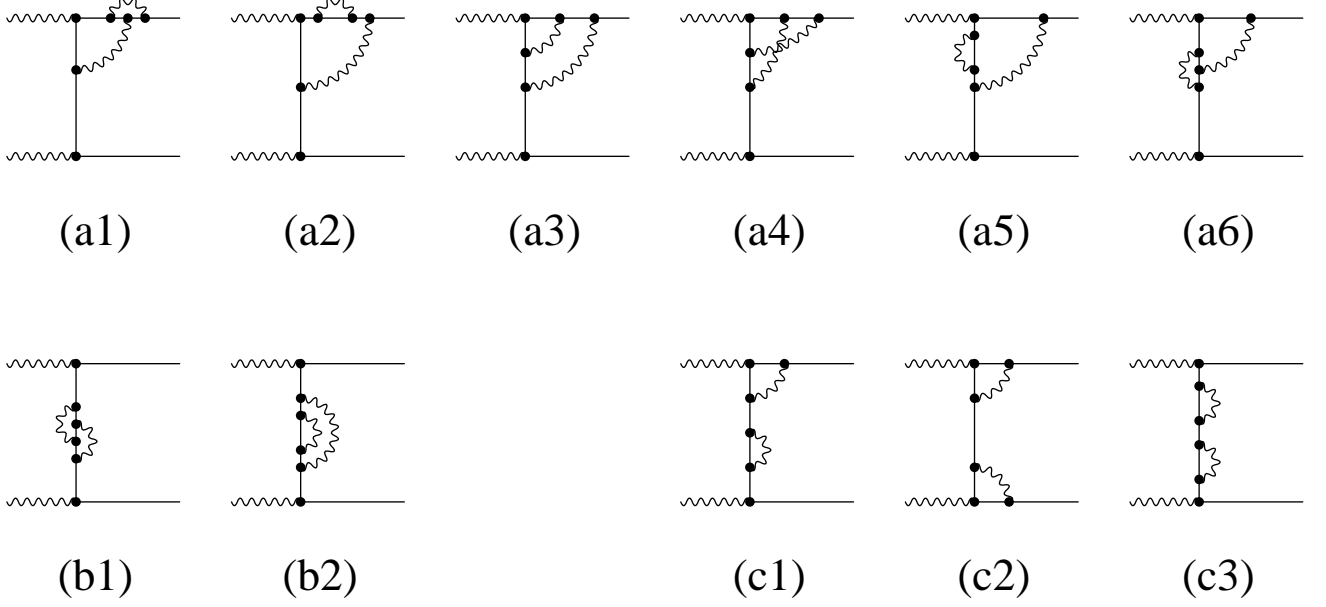


FIG. 6: Contribution to the p-Ps decay rate from groups a (the two-loop vertex corrections), b (the two-loop self-energy corrections), and c (products of one-loop vertex and self-energy parts).

$$I'_a = \frac{1}{8\epsilon^2} + \frac{1}{\epsilon} \left(\frac{\pi^2}{16} - \ln 2 - \frac{3}{16} \right) + 2.8841255(52). \quad (54)$$

This is renormalized according to

$$I_a = I'_a - \ell_1 I'_V - 4(\tilde{\ell}_2 - \ell_1^2) I^{(0)}, \quad (55)$$

where

$$I'_V = \frac{1}{\epsilon} + \left(\frac{\pi^2}{4} - 4 \ln 2 \right) + \epsilon \left(\frac{7}{2} \zeta(3) + \frac{\pi^2}{4} + 4 \ln^2 2 - 8 \ln 2 \right) + O(\epsilon^2) \quad (56)$$

is the unrenormalized one-loop vertex correction (see Fig. 5); $L_1 = (\alpha/\pi)\ell_1$, where

$$\ell_1 = \frac{1}{4\epsilon} + (\ln \lambda + 1) + \epsilon \left(-\ln^2 \lambda + \frac{\pi^2}{48} + 2 \right) + O(\epsilon^2), \quad (57)$$

is the one-loop vertex renormalization constant; and $\tilde{L}_2 = (\alpha/\pi)^2 \tilde{\ell}_2$, where

$$\tilde{\ell}_2 = \frac{1}{32\epsilon^2} + \frac{1}{\epsilon} \left(\frac{\ln \lambda}{4} + \frac{13}{64} \right) + \left(\frac{1}{4} \ln^2 \lambda + \ln \lambda + \frac{3}{2} \zeta(3) - \pi^2 \ln 2 + \frac{157\pi^2}{192} - \frac{49}{128} \right) + O(\epsilon), \quad (58)$$

is the two-loop renormalization constant (with the vacuum polarization effect excluded).

Because we treat vacuum polarization separately, it is important to again emphasize that the renormalization constant above also does not include the effect of vacuum polarization.

Our result for the two-loop renormalized class a contribution is

$$I_a = -2 \ln^2 \lambda - \ln \lambda I_V(\lambda) - 1.966447(6), \quad (59)$$

where $I_V(\lambda)$ is the one-loop vertex factor of Eq. (49).

Turning to the two-loop self-energy diagrams, shown in Fig. 6b, we again present results with self-mass counterterms understood. The unrenormalized results are given in Table II and are in agreement, after accounting for the different convention, with CMY. The total class b unrenormalized result is

$$I'_b = -\frac{1}{16\epsilon^2} + \frac{1}{\epsilon} \left(\ln 2 - \frac{5}{32} \right) - 1.6727038(15). \quad (60)$$

The corresponding renormalized expression is

$$\begin{aligned} I_b &= I'_b - \ell_1 I'_{SE} + 2(\tilde{\ell}_2 - \ell_1^2) \\ &= \ln^2 \lambda - \ln \lambda I_{SE}(\lambda) - 2.0277430(15), \end{aligned} \quad (61)$$

where I'_{SE} is the unrenormalized one-loop self-energy correction

$$I'_{SE} = -\frac{1}{2\epsilon} + (4 \ln 2 - 1) + \epsilon \left(\frac{7\pi^2}{24} - 4 \ln^2 2 + 6 \ln 2 - 2 \right) + O(\epsilon^2), \quad (62)$$

and $I_{SE}(\lambda)$ is the renormalized one-loop self-energy factor of Eq. (48).

The diagrams with two separate one-loop corrections shown in Fig. 6c are simple to evaluate and can be done entirely analytically. The breakdown of the calculation is given in Table III and agrees exactly with CMY. Interestingly, the total class c contribution is unchanged by renormalization. It is

$$I_c = \frac{\pi^4}{128} + \frac{1}{4}\pi^2 \ln 2 - \frac{\pi^2}{8} + \ln^2 2 - \ln 2 + \frac{1}{4}. \quad (63)$$

The least complicated contributions are those, shown in Fig. 7d, which have no ultraviolet or infrared divergences. The results, given in Table IV, can be directly compared with the diagrams called D_{14} and D_3 by CMY and are in agreement. For the class d total we find

$$I_d = -0.87783(7). \quad (64)$$

The vacuum polarization diagrams of Fig. 7e were evaluated in Refs. [30, 31], with result

$$I_e = 0.4473430(6). \quad (65)$$

As with o -Ps, by far the most difficult diagrams to treat were those of class f, with at least one binding photon exchanged. As before, the most infrared singular contributions are

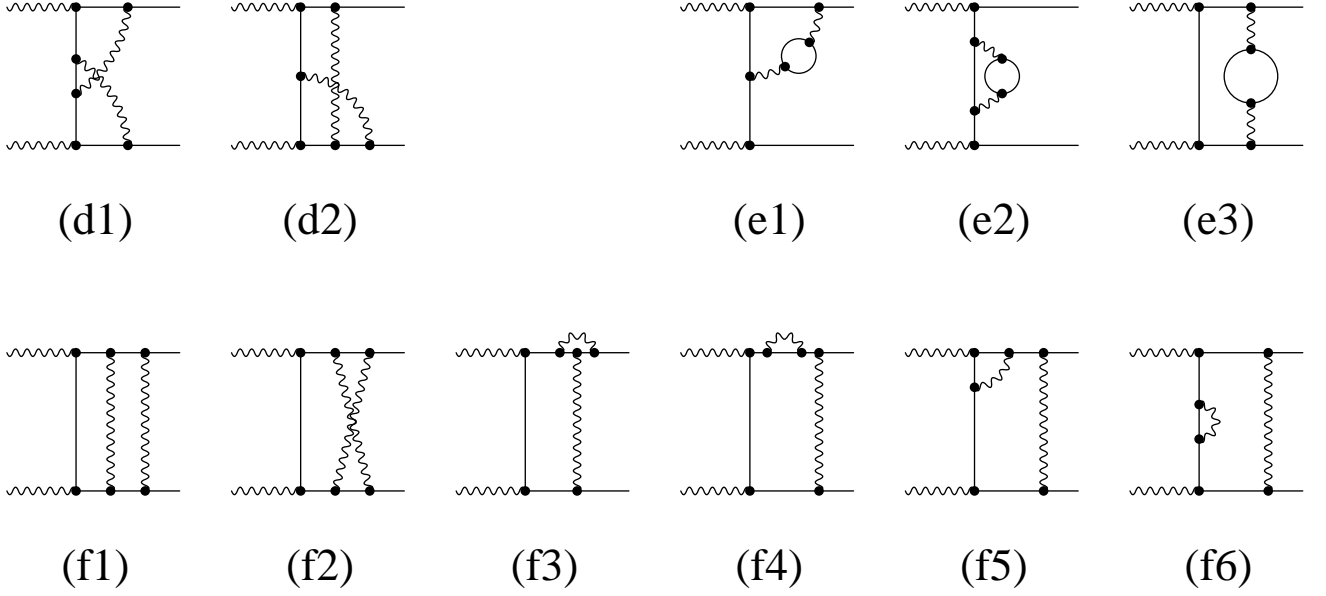


FIG. 7: Contribution to the p-Ps decay rate from groups d (infrared and ultraviolet finite contributions), e (vacuum polarization corrected one-loop graphs), and f (ladder graphs).

the ladder and crossed-ladder f1 and f2. They were treated just as in the *o*-Ps calculation by subtracting off the most infrared singular part of each (called f1a0 and f2a0), which were evaluated as a unit. We found that

$$I_{f1} = I_{f1a0} + I_B(\lambda)I_{LS}(\lambda) - 3\pi^2 \ln \lambda - 55.2277(15), \quad (66)$$

$$I_{f2} = I_{f2a0} + \pi^2 \ln \lambda + 30.8346(7), \quad (67)$$

where (see Eq. (51)) $I_{LS} \equiv I_L - 2I_B = O(\lambda)$. The leading binding singularity is contained in

$$I_{f1a0} + I_{f2a0} = 2I^{a0} = \frac{2\pi^2 \ln 2}{\lambda^2} + 2\left(I_B - \frac{\pi}{\lambda}\right)\frac{\pi}{\lambda} + \ln^2 \lambda - 2 \ln \lambda + 2A_0, \quad (68)$$

where

$$A_0 = -3.2036(13) \quad (69)$$

as given in Eqs. (3.37) and (3.86) of [13]. Diagrams f3 and f4 were evaluated using Yennie gauge for the vertex or self-energy photon and Feynman gauge for the ladder photon. This procedure is consistent since the sum of the two is independent of the gauge of the vertex or self-energy photon. An all-Feynman-gauge evaluation of f3 and f4 proved to be numerically difficult. The class f results are given in Table V. The total class f contribution is

$$I_f = \frac{2\pi^2 \ln 2}{\lambda^2} + \frac{\pi}{\lambda}A(\lambda) + \ln^2 \lambda + (I_V(\lambda) + I_{SE}(\lambda) - 2\pi^2) \ln \lambda - 35.0357(32). \quad (70)$$

Class g is the set of energy shift contributions having one-loop corrections (SE, V, or L) both before and after the annihilation into two photons. This contribution is easily evaluated as the square of half the one-loop correction:

$$I_g = \left[\frac{1}{2} I^{(1)} \right]^2 = \frac{\pi^2}{\lambda^2} + \frac{\pi}{\lambda} A(\lambda) + \left(\frac{\pi^2}{8} - \frac{5}{2} \right)^2. \quad (71)$$

Finally, class h represents the effect of light-by-light scattering on the annihilation photons. This contribution was evaluated in Ref. [29] to be

$$I_h = 1.29392(4). \quad (72)$$

The total two-loop contribution is then

$$I^{(2)} = \frac{\pi^2(2 \ln 2 + 1)}{\lambda^2} + \frac{2\pi}{\lambda} A(\lambda) - 2\pi^2 \ln \lambda + B_2, \quad (73)$$

with

$$B_2 = -35.2881(33). \quad (74)$$

The total QED scattering amplitude at threshold through two-loop order is the sum of the $M_{QED}^{(i)}$ for i equal to 0, 1, and 2.

Most of the two-loop results can be cross-checked against corresponding results of CMY as given in Ref. [14]. This comparison is detailed in Table VII. The a graphs can be compared directly to the corresponding CMY graphs except for a2 and a5, whose CMY counterparts D_{11} and D_{12} require the inclusion of the one-loop self-mass $\delta m^{(1)}$ as given in CMY Eq. (48). (For ease of notation we take $m \rightarrow 1$ in the CMY expressions for δm .) The CMY counterparts of the b graphs require one- and two-loop self-mass insertions. It is necessary to isolate the “crossed rainbow” and “double rainbow” contributions to $\delta m^{(2)}$, which are

$$\delta m_{CR}^{(2)} = -\frac{3}{\epsilon^2} - \frac{5}{2\epsilon} - 12\zeta(3) + 8\pi^2 \ln 2 - \frac{9\pi^2}{2} + \frac{1}{4}, \quad (75)$$

$$\delta m_{DR}^{(2)} = \frac{15}{2\epsilon^2} + \frac{55}{4\epsilon} + \frac{\pi^2}{4} + \frac{197}{8}, \quad (76)$$

as given in Ref. [32] but adapted to the conventions of CMY. The c graphs were done analytically by both groups, and agree exactly once appropriate self-mass insertions are made. The d graphs are directly comparable. The e (vacuum polarization) graphs were taken from Ref. [31] by both groups. The f graphs, which involve the binding interaction, were the most difficult to compare. In fact, the double ladder and crossed ladder graphs

f1 and f2 could not be checked against their CMY counterparts D_4 and D_1 because the methods for regulating the binding singularities were completely different. We evaluated graphs f3 and f4 with Yennie gauge vertex and self-energy photons, but the sum is directly comparable with $D_2 + D_5$ of CMY after the appropriate self-mass correction is made to their result. The comparison for f5 and f6 is a bit more delicate. For the sum f5+f6 we found

$$I_{f5} + I_{f6} = (I_V + I_{SE})I_B + 1.29396(4), \quad (77)$$

where I_V and I_{SE} are the renormalized vertex and self-energy corrections. Now CMY calculate unrenormalized graphs, so we revert to the unrenormalized contribution as well: $I_V + I_{SE} \rightarrow I'_V + I'_{SE}$, where in CMY notation

$$I'_V + I'_{SE} = 4(S_2 + S_3 + \delta m^{(1)} B_1). \quad (78)$$

Now I_B is half the contribution of the one-loop ladder graph, which in CMY terms is $I_B = (4S_1)/2 = 2S_1$. Note that we must regulate the infrared divergence via dimensional regulation for purposes of comparison, since that is the method of CMY. Now the sum $I_{f5} + I_{f6}$, with the substitutions for $I_V + I_{SE}$ and I_B discussed above, is given by

$$I_{f5} + I_{f6} \rightarrow \frac{1}{4\epsilon^2} + \frac{1}{\epsilon} \left(\frac{\pi^2}{8} - 1 \right) + 5.84851(4), \quad (79)$$

while the corresponding CMY contribution is

$$D_6 + D_7 + \delta m^{(1)} C_7 = \frac{1}{4\epsilon^2} + \frac{1}{\epsilon} \left(\frac{\pi^2}{8} - 1 \right) + 5.850(12). \quad (80)$$

IV. RESULTS AND CONCLUSION

The NRQED couplings e_1 and e_2 are determined by requiring agreement between the imaginary parts of the scattering amplitude as calculated by NRQED and QED. The NRQED version of this amplitude, given in Eq. (43), is

$$\begin{aligned} M_{NRQED} = & V_4^0 \left\{ \left[1 + \frac{\alpha}{\pi} e_1 + \left(\frac{\alpha}{\pi} \right)^2 e_2 \right] + \frac{\alpha}{\pi} \left[\frac{2\pi}{\lambda} \left(1 + \frac{\alpha}{\pi} e_1 \right) - \frac{2\Lambda}{3m} + \frac{7\pi\lambda}{12} \right] \right. \\ & \left. + \left(\frac{\alpha}{\pi} \right)^2 \left[\frac{\pi^2(2\ln 2 + 1)}{\lambda^2} - \frac{4\pi\Lambda}{3\tilde{\lambda}} + 2\pi^2 \ln \left(\frac{\Lambda}{2\tilde{\lambda}} \right) + \frac{4\pi^2}{3} \right] \right\}. \end{aligned} \quad (81)$$

The corresponding QED version is

$$\begin{aligned} M_{QED} = & V_4^0 \left\{ 1 + \frac{\alpha}{\pi} \left[\frac{2\pi}{\lambda} + A(\lambda) \right] \right. \\ & \left. + \left(\frac{\alpha}{\pi} \right)^2 \left[\frac{\pi^2(2\ln 2 + 1)}{\lambda^2} + \frac{2\pi}{\lambda} A(\lambda) - 2\pi^2 \ln \lambda + B_2 \right] \right\}. \end{aligned} \quad (82)$$

Matching at the one-loop (order α) level yields

$$e_1 = \frac{2\Lambda}{3m} + A(\lambda) - \frac{7\pi\lambda}{12}. \quad (83)$$

To order $\alpha\Gamma_0$, this value of e_1 used in Eq. (31) cancels the ultraviolet divergent term and reproduces the Harris-Brown result [19] after taking the limit $\lambda \rightarrow 0$. Matching at the two-loop (order α^2) level gives

$$e_2 = -2\pi^2 \ln\left(\frac{\Lambda}{2m}\right) - \frac{\pi^2}{6} + B_2. \quad (84)$$

Care is required with the photon mass λ in this evaluation. While it is ultimately taken to vanish, we keep it in e_1 because that factor enters as a factor of $1/\lambda$ terms. However, while e_2 also has terms proportional to the photon mass, they can be dropped because we do not need the next renormalization constant e_3 , which enters in higher order. We note that the uncalculated $O(\lambda)$ part of $A(\lambda)$ cancels from the calculation.

With e_1 and e_2 now determined from the matching calculation, we return to the bound state NRQED calculation and use these values in Eq. (31). Taking the limit $\lambda \rightarrow 0$ then gives our final result for the two photon decay rate through two-loop order:

$$\Gamma_{\text{NRQED}} = \left\{ 1 + \frac{\alpha}{\pi} \left(\frac{\pi^2}{4} - 5 \right) + \left(\frac{\alpha}{\pi} \right)^2 [-2\pi^2 \ln \alpha + B_{2\gamma}] \right\} \Gamma_0, \quad (85)$$

where

$$B_{2\gamma} = B_2 + \frac{65\pi^2}{24} + 2\pi^2 \ln 2 = 5.1243(33). \quad (86)$$

As noted in the introduction, this is consistent with the CMY result. Inclusion of all known contributions leads to

$$\Gamma_{p\text{-Ps}} = \left\{ 1 + A \frac{\alpha}{\pi} - 2\alpha^2 \ln \alpha + B \left(\frac{\alpha}{\pi} \right)^2 - \frac{3\alpha^3}{2\pi} \ln^2 \alpha + C \frac{\alpha^3}{\pi} \ln \alpha + D \left(\frac{\alpha}{\pi} \right)^3 \right\} \Gamma_0, \quad (87)$$

where $A = \pi^2/4 - 5$,

$$B = B_{2\gamma} + B_{4\gamma} = 5.3986(33), \quad (88)$$

$C = 7.9189$, and D is uncalculated. Our final numerical result is

$$\Gamma_{p\text{-Ps}} = 7989.6178(2) \mu s^{-1}. \quad (89)$$

The uncalculated D term makes a contribution of $0.00010D\mu s^{-1}$. Numerical contributions of the various terms in $\Gamma_{p\text{-Ps}}$ are detailed in Table VIII. While the experimental precision is

relatively high for a decay measurement, it is far too low to be sensitive to the precise value of B , only disfavoring a very large value on the order of 50 or more. The very short lifetime of the state makes it unlikely that significant improvements in the experimental precision can be achieved in the near future.

We consider one of the most important aspects of the present calculation to be its impact on the decay rate of o -Ps. We have applied exactly the same methods to both decay rates. In the o -Ps case, while no independent check of our calculation was then, or is now, available, we did use the same implementation of NRQED to calculate a contribution to the ground state hyperfine splitting of positronium that had been determined using Coulomb gauge Bethe-Salpeter methods [33] and additionally an independent NRQED approach [34], finding good agreement. This indirect confirmation of the validity of our methods has now been further buttressed by the fact that we have agreement for the decay rate of p -Ps with CMY, who, as we have emphasized above, use an entirely different implementation of NRQED. Therefore, the confrontation of QED with experiment in this system, summarized as

$$\begin{aligned}
\Gamma_{o\text{-Ps}}^{th}[13] &= 7.039979(11)\mu s^{-1} \\
\Gamma_{o\text{-Ps}}^{exp}[35] &= 7.0514(14)\mu s^{-1} \\
\Gamma_{o\text{-Ps}}^{exp}[36] &= 7.0482(16)\mu s^{-1} \\
\Gamma_{o\text{-Ps}}^{exp}[37] &= 7.0398(29)\mu s^{-1}
\end{aligned} \tag{90}$$

remains in an unresolved state, and strongly indicates the need for further experimental work.

Acknowledgments

The work of JS was partially supported by NSF grant PHY-0097641, and that of GA by NSF grant PHY-0070819. GA acknowledges the hospitality of the Physics department of UCLA. The constant encouragement of the Michigan experimental group is gratefully acknowledged.

[1] U. van Kolck, Nucl. Phys. A **699**, 33 (2002).

- [2] A.S. Kronfeld, in *At the Frontiers of Physics: Handbook of QCD*, edited by M. Shifman (World Scientific, Singapore, 2002), Vol 4.
- [3] A.V. Manohar and M.B. Wise, *Heavy Quark Physics*, (Cambridge University Press, New York, 2000).
- [4] E. Braaten, H.-W. Hammer, and T. Mehen, Phys. Rev. Lett. **88**, 040401 (2002).
- [5] W.E. Caswell and G.P. Lepage, Phys. Lett. **167B**, 437 (1986).
- [6] E.E. Salpeter and H.A. Bethe, Phys. Rev. **84**, 1232 (1951).
- [7] G.P. Lepage, Phys. Rev. A **16**, 863 (1977).
- [8] G.T. Bodwin and D.R. Yennie, Phys. Rep **43**, 267 (1978).
- [9] G.S. Adkins and R.N. Fell, Phys. Rev. A **60**, 4461 (1999).
- [10] K. Pachucki, Phys. Rev. Lett. **84**, 4561 (2000); A. Yelkhovsky, Phys. Rev. A **64**, 062104 (2001).
- [11] K. Pachucki, Phys. Rev. A **56**, 297 (1997); A.H. Hoang, P. Labelle, and S.M. Zebarjad, Phys. Rev. A **62**, 012109 (2000).
- [12] M. Nio and T. Kinoshita, Phys. Rev. D **55**, 7267 (1997).
- [13] G.S. Adkins, R.N. Fell, and J. Sapirstein, Ann. Phys. (N.Y.) **295**, 136 (2002).
- [14] A. Czarnecki, K. Melnikov, and A. Yelkhovsky, Phys. Rev. A **61**, 052502 (2000); **62**, 059902(E) (2000).
- [15] J.A. Wheeler, Ann. N.Y. Acad. Sci. **48**, 219 (1946).
- [16] J. Pirenne, Arch. Sci. Phys. Nat. **29**, 265 (1947).
- [17] P.J. Mohr and B.N. Taylor, Rev. Mod. Phys. **72**, 351 (2000).
- [18] A.H. Al-Ramadhan and D.W. Gidley, Phys. Rev. Lett. **72**, 1632 (1994).
- [19] I. Harris and L.M. Brown, Phys. Rev. **105**, 1656 (1957).
- [20] A.P. Mills and S. Berko, Phys. Rev. Lett. **18**, 420 (1967).
- [21] P.A. Vetter and S.J. Freedman, Phys. Rev. A **66**, 052505 (2002).
- [22] A. Billoire, R. Lacaze, A. Morel, and H. Navelet, Phys. Lett. B **78**, 140 (1978).
- [23] G.S. Adkins and E.D. Pfahl, Phys. Rev. A **59**, R915 (1999).
- [24] I.B. Khriplovich and A.S. Yelkhovsky, Phys. Lett. B **246**, 520 (1990).
- [25] S.G. Karshenboim, Zh. Eksp. Teor. Fiz. **103**, 1105 (1993) [JETP **76**, 541 (1993)].
- [26] R.J. Hill and G.P. Lepage, Phys. Rev. D **62**, 111301 (2000).
- [27] B.A. Kniehl and A.A. Penin, Phys. Rev. Lett. **85**, 1210 (2000); **85**, 3065(E) (2000).

- [28] K. Melnikov and A. Yelkhovsky, Phys. Rev. D **62**, 116003 (2000).
- [29] G.S. Adkins, R.N. Fell, and J. Sapirstein, Phys. Rev. A **63**, 032511 (2001).
- [30] A.P. Burichenko and D.Y. Ivanov, Yad. Fiz. **58**, 898 (1995) [Phys. At. Nucl. **58**, 832 (1995)].
- [31] G.S. Adkins and Y. Shiferaw, Phys. Rev. A **52**, 2442 (1995).
- [32] G.S. Adkins, R.N. Fell, and J. Sapirstein, Phys. Rev. D **63**, 125009 (2001).
- [33] G.S. Adkins, R.N. Fell, and P.M. Mitrikov, Phys. Rev. Lett. **79**, 3383 (1997).
- [34] A.H. Hoang, P. Labelle, and S.M. Zebarjad, Phys. Rev. Lett. **79**, 3387 (1997).
- [35] C.I. Westbrook, D.W. Gidley, R.S. Conti, and A. Rich, Phys. Rev. A **40**, 5489 (1989).
- [36] J.S. Nico, D.W. Gidley, A. Rich, and P.W. Zitzewitz, Phys. Rev. Lett. **65**, 1344 (1990).
- [37] S. Asai, S. Orito, and N. Shinohara, Phys. Lett. B **357**, 475 (1995).

TABLE I: Unrenormalized contributions to the parapositronium decay rate from class a. Class a consists of two-loop vertex corrections.

diagram	$\frac{1}{\epsilon^2}$	$\frac{1}{\epsilon}$	1
a1	$\frac{1}{8}$	$\frac{\pi^2}{16} - \ln 2 + \frac{3}{16}$	-0.3237469(14)
a2	$-\frac{1}{8}$	$-\frac{\pi^2}{16} + \ln 2 - \frac{3}{16}$	-0.3245758(11)
a3	$\frac{1}{8}$	$\frac{\pi^2}{16} - \ln 2 + \frac{5}{16}$	1.4769869(20)
a4	0	$-\frac{1}{2}$	3.492237(3)
a5	$-\frac{1}{8}$	$-\frac{\pi^2}{16} + \ln 2 - \frac{3}{16}$	-1.330000(3)
a6	$\frac{1}{8}$	$\frac{\pi^2}{16} - \ln 2 + \frac{3}{16}$	-0.1067757(12)
total	$\frac{1}{8}$	$\frac{\pi^2}{16} - \ln 2 - \frac{3}{16}$	2.8841255(52)

TABLE II: Unrenormalized contributions to the parapositronium decay rate from class b. Class b consists of two-loop self-energy corrections.

diagram	$\frac{1}{\epsilon^2}$	$\frac{1}{\epsilon}$	1
b1	$-\frac{1}{8}$	$2 \ln 2 - \frac{7}{16}$	-1.4022755(10)
b2	$\frac{1}{16}$	$-\ln 2 + \frac{9}{32}$	-0.2704283(10)
total	$-\frac{1}{16}$	$\ln 2 - \frac{5}{32}$	-1.6727038(15)

TABLE III: Unrenormalized contributions to the parapositronium decay rate from class c. Class c consists of products of two one-loop vertex or self-energy corrections.

diagram	$\frac{1}{\epsilon^2}$	$\frac{\pi^2}{\epsilon}$	$\frac{\ln 2}{\epsilon}$	$\frac{1}{\epsilon}$	π^4	$\zeta(3)$	$\pi^2 \ln 2$	π^2	$\ln^2 2$	$\ln 2$	1
c1	$-\frac{1}{4}$	$-\frac{1}{16}$	3	$-\frac{1}{2}$	0	$-\frac{7}{8}$	$\frac{1}{2}$	$-\frac{1}{24}$	-7	6	-1
c2	$\frac{1}{8}$	$\frac{1}{16}$	-1	0	$\frac{1}{128}$	$\frac{7}{8}$	$-\frac{1}{4}$	$\frac{1}{16}$	2	-2	0
c3	$\frac{1}{8}$	0	-2	$\frac{1}{2}$	0	0	0	$-\frac{7}{48}$	6	-5	$\frac{5}{4}$
total	0	0	0	0	$\frac{1}{128}$	0	$\frac{1}{4}$	$-\frac{1}{8}$	1	-1	$\frac{1}{4}$

TABLE IV: Contributions to the parapositronium decay rate from class d. Class d consists of ultraviolet and infrared finite two-loop corrections.

diagram	1
d1	-0.80394(3)
d2	-0.07389(6)
total	-0.87783(7)

TABLE V: Contributions to the parapositronium decay rate from class f. Class f contains the ladder graphs.

diagram	$I_B(\lambda)$	$\pi^2 \ln \lambda$	1
f1-f1a0	$I_{LS}(\lambda)$	-3	-55.2277(15)
f2-f2a0	0	1	30.8346(7)
f3	0	0	-10.05855(11)
f4	0	0	3.9965673(13)
f5	$I_V(\lambda)$	0	1.94968(4)
f6	$I_{SE}(\lambda)$	0	-0.655722(5)
total	$I_{LS}(\lambda) + I_V(\lambda) + I_{SE}(\lambda)$	-2	-29.1611(17)

TABLE VI: Renormalized two-loop QED contributions to the parapositronium decay rate by class.

class	$\frac{\pi^2}{\lambda^2}$	$\frac{\pi}{\lambda}$	$\ln^2 \lambda$	$\ln \lambda$	1
a	0	0	-2	$-I_V(\lambda)$	-1.966447(6)
b	0	0	1	$-I_{SE}(\lambda)$	-2.0277430(15)
c	0	0	0	0	1.274886
d	0	0	0	0	-0.87783(7)
e	0	0	0	0	0.4473430(6)
f	$2 \ln 2$	$A(\lambda)$	1	$I_V(\lambda) + I_{SE}(\lambda) - 2\pi^2$	-35.0357(32)
g	1	$A(\lambda)$	0	0	1.603514
h	0	0	0	0	1.29392(4)
total	$2 \ln 2 + 1$	$2A(\lambda)$	0	$-2\pi^2$	-35.2881(33)

TABLE VII: Cross-check of results between this work (AMFS) and CMY. The $1/\epsilon^2$ and $1/\epsilon$ terms agree analytically in all cases, only the finite parts are displayed. The comparison for f5+f6 is subtle and is discussed in the text.

AMFS	CMY	AMFS	CMY	Difference
Graph	Graph	Result	Result	AMFS-CMY
a1	D_8	-0.3237469(14)	-0.324(1)	0.000(1)
a2	$D_{11} + \delta m^{(1)} C_{11}$	-0.3245758(11)	-0.33(3)	0.01(3)
a3	D_9	1.4769869(20)	1.475(50)	0.00(5)
a4	D_{10}	3.492237(3)	3.488(2)	0.004(2)
a5	$D_{12} + \delta m^{(1)} C_{12}$	-1.330000(3)	-1.27(12)	-0.06(12)
a6	D_{13}	-0.1067757(12)	-0.12(1)	0.01(1)
b1	$D_{16} + \delta m_{CR}^{(2)} B_1$	-1.4022755(10)	-1.403(4)	0.001(4)
b2	$D_{17} + \delta m^{(1)} C_{17} + \delta m_{DR}^{(2)} B_1$	-0.2704283(10)	-0.271(1)	0.001(1)
c1	$D_{19} + \delta m^{(1)} C_{19}$	analytic	analytic	0
c2	D_{18}	analytic	analytic	0
c3	$D_{15} + \delta m^{(1)} C_{15} + (\delta m^{(1)})^2 B_2$	analytic	analytic	0
d1	D_{14}	-0.80394(3)	-0.804(2)	0.000(2)
d2	D_3	-0.07389(6)	-0.074(2)	0.000(2)
f3+f4	$D_2 + D_5 + \delta m^{(1)} C_5$	-6.06198(11)	-6.03(20)	-0.03(20)
f5+f6	$D_6 + D_7 + \delta m^{(1)} C_7$	5.84851(4)	5.850(12)	-0.001(12)

TABLE VIII: Numerical values of contributions to the parapositronium decay rate.

term	contribution (in μs^{-1})
1	8032.5028(1)
$A\frac{\alpha}{\pi}$	-47.2534
$-2\alpha^2 \ln \alpha$	4.2092
$B(\frac{\alpha}{\pi})^2$	0.2340(1)
$-\frac{3\alpha^3}{2\pi} \ln^2 \alpha$	-0.0361
$C\frac{\alpha^3}{\pi} \ln \alpha$	-0.0387
$D(\frac{\alpha}{\pi})^3$	0.00010 D
total	7989.6178(2) + 0.00010D